Catalysis Letters, Vol. 114, Nos. 3–4, April 2007 (© 2007)
DOI: 10.1007/s10562-007-9060-6

Effect of manganese on a potassium-promoted iron-based Fischer-Tropsch synthesis catalyst

Zhichao Tao,[a,b] Yong Yang,[a] Haijun Wan,[a,b] Tingzhen Li,[a,b] Xia An,[a,b] Hongwei Xiang,[a,*] and Yongwang Li[a]

[a]*State Key Laboratory of Coal Conversion, Institute of Coal Chemistry, Chinese Academy of Sciences, Taiyuan, 030001, People's Republic of China*
[b]*Graduate University of Chinese Academy of Sciences, Beijing, 100039, People's Republic of China*

Received 22 November 2006; accepted 16 January 2007

The effects of manganese promoter on the reduction–carburization behavior, surface basicity, bulk phase structure and their correlation with Fischer-Tropsch synthesis (FTS) performances have been emphatically studied over a series of spray-dried Fe–Mn–K catalysts with a wide range of Mn incorporation amount. The catalysts were characterized by means of H_2 and CO temperature-programmed reduction (TPR), CO_2 temperature-programmed desorption (TPD), Mössbauer spectroscopy etc.. The results indicated that small amount of Mn promoter can promote the reduction of the catalyst in H_2. However, FeO phase formed during reduction is stabilized by MnO phase with the further increase of Mn content, making FeO phase difficult to be reduced in H_2. The addition of Mn promoter can stabilize the Fe^{2+} and Fe^{3+} ions, and suppresses the reduction and carburization of the catalyst in syngas and CO. Mn promoter can also enhance the amount of the basic sites and weaken the strength of the basic sites, which possibly come from the reason that the Mn–K interaction is strengthened with the addition of Mn promoter. The change of surface basicity can modify the selectivity of hydrocarbons and olefins, and the change of bulk structure phase derived from the addition of Mn promoter will affect the catalyst activity and run stability. The synergetic effects of the two main factors result in an optimized amount of Mn promoter for the highest catalyst activity and heavy hydrocarbon selectivity in slurry FTS reaction of Fe–Mn–K catalysts.

KEY WORDS: Fischer-Tropsch synthesis; iron–manganese catalyst; manganese promoter.

1. Introduction

Fischer-Tropsch synthesis (FTS) is a well-established catalytic process to convert syngas (H_2 and CO) derived from coal or natural gas to transportation fuels and petrochemical substitutes [1–4]. The iron-based catalysts are often used in the commercial operations, especially for coal derived syngas with low H_2/CO ratio, due to their high water gas shift (WGS) activity, low cost, flexible operation conditions as well as reasonable products distribution [5–8].

To improve FTS performances (activity, selectivity and stability) of iron-based catalyst, lots of efforts have been performed on the addition of electronic or structural promoters [9]. Typical iron-based catalysts often incorporated with more or less potassium as an electronic promoter. It is believed that potassium can improve the dissociation adsorption of CO and increase both FTS and WGS catalytic activities [3,5,10,11]. It is also reported that potassium can increase the selectivity to olefin and suppress the formation of methane [12,13]. However, excessive potassium can facilitate carbon deposition and induce catalyst deactivation [12,14].

Manganese also has been widely used as one of the promoters for iron-based FTS catalyst. It is reported that manganese can decrease the methane selectivity and promote the formation of olefin, even at a high Fe/Mn ratio [15–17]. Mn promoter can also improve the dispersion of α-Fe_2O_3 and suppress the chain growth as well as deep hydrogenation of primary FTS products, which also lead to high selectivity to light olefins [18]. Comparing with the classical potassium-promoted precipitated iron catalysts, iron–manganese catalysts possess high yield of C_{2-4} olefins [19]. However, as an electronic promoter, manganese is an electron-donating promoter, like potassium, promotes dissociation adsorption of CO and increases the selectivity of olefin in gas phase, and shifts the products to heavy hydrocarbons [19,20]. Mn promoter also promotes the formation of amorphous or graphitic carbon and leads to catalyst deactivation [21]. On the other hand, it is found that Mn has some structural promotion and stabilizes the iron-based catalyst [22,23], and the structural promotion also plays an important role in the catalytic performances [24]. When Mn acts at a structural promoter, the chemisorptive properties of the catalyst are affected due to the strong metal support interaction (SMSI) effect, which promotes the transformation of syngas into light olefins [20,21]. Thereby, it is considerable to introduce Mn promoter into the Fe–K catalyst system, in order to stabilize the catalyst and optimize the products distribution.

*To whom correspondence should be addressed.
E-mail: hwxiang@sxicc.ac.cn

Many previous studies for Mn promotion were focused on the effects of Mn on phase structure during reduction and FTS process, activity and hydrocarbon distribution over K-free Fe–Mn catalyst. However, the effect of Mn on the reduction–carburization behavior, surface basicity, bulk phase structure and their correlation over K-promoted Fe–Mn catalyst is rarely mentioned. These are inherent factors to decide the catalytic performance (activity, stability, adsorption behavior and selectivity). Moreover, almost all the iron–manganese catalysts of the previous studies are reduced in H_2, little results have been reported on the reduction and carburization behavior in syngas. Therefore, it is very necessary to perform a systematic study of the effect of manganese over a K-promoted Fe–Mn catalyst.

The present work was undertaken to develop a systematic understanding of the effect of manganese over a precipitated Fe–Mn catalyst promoted with potassium under industrial operation conditions. Particular attentions were paid to the effect of manganese promoter on the interactions among iron, manganese and potassium, the reduction/carburization behavior, the surface basicity and the bulk phase structure of the catalyst. FTS activity, stability and the hydrocarbon selectivity were systematically investigated and well correlated with the characterization results.

2. Experimental

2.1. Catalyst preparation

The catalysts used in this study were prepared by the combination of co-precipitated and spray drying method. The detailed preparation method has been described elsewhere [25]. Briefly, a solution containing $Fe(NO_3)_3$ and $Mn(NO_3)_2$ with the desired ratio was coprecipitated with NH_4OH solution as precipitator at pH = 9.0 ± 0.1 and T = 80 ± 1 °C. The precipitate was completely washed, and then filtered. Required amounts of K_2CO_3 solution were subsequently added into the precipitate, and the mixture was re-slurried and spray-dried. The spray-dried powder was finally calcined at 500 °C for 5 h in a muffle furnace, and got fresh catalyst samples with spherical particle size of 10–20 μm for the application of FTS in slurry reactor. The weight ratio of $K_2O/(Fe_2O_3 + Mn_2O_3)$ and Mn/Fe for these fresh catalysts are 0.012 and 0–3, respectively. In addition, a Fe-free model catalyst was also prepared used the same method for well comparing study. The composition and label of the catalysts used in this study are presented in table 1.

2.2. Catalyst characterizations

The elemental contents in the catalysts were determined by inductively coupled plasma emission spectroscopy (ICPES) using an Atomscan 16 spectrometer (TJA, USA).

Powder X-ray diffraction (XRD) measurements were carried out on a D/max-RA X-ray diffractometer (Rigaku, Japan), equipped with CuKα radiation ($\lambda = 1.5406$Å) at 40 kV and 150 mA.

H_2 temperature-programmed reduction (TPR) experiment was performed in a conventional atmospheric quartz flow reactor (5 mm i.d.). A flow of 5%H_2/Ar (on mole basis), maintained at a flow of 50 mL/min, was used as the reduction gas, and the TPR profiles were recorded by using the response of the thermal conductivity detector (TCD) of the effluent gas. Typically, 40 mg samples were loaded and reduced by 5 %H_2/Ar with the temperature rising from 100 °C to 800 °C at a rate of 6 °C/min.

CO temperature-programmed reduction (TPR) experiment was performed in the same equipment and used the same condition with that of the H_2-TPR. A flow of 5%CO/He (on mole basis), maintained at a flow of 50 ml/min, was used as the reduction gas, and an in-line liquid-nitrogen trap, located between the reactor and the TCD, was used to remove CO_2 produced during reduction.

CO_2 temperature-programmed desorption (TPD) was performed using the same equipment with that of the TPR measurements. Typically, 200 mg samples were

Table 1
Detailed composition and label of the catalysts used in the study

Catalysts	Nominal composition (by weight)		Analyzed composition (by weight)	
	Fe/Mn/K	$K_2O/(Fe_2O_3 + Mn_2O_3) \times 100$	Fe/Mn/K	$K_2O/(Fe_2O_3 + Mn_2O_3) \times 100$
Mn0	100Fe/0Mn/1.4K	1.2	100Fe/0Mn/1.5K	1.2
Mn6	100Fe/6Mn/1.5K	1.2	100Fe/7.5Mn/1.6K	1.2
Mn12	100Fe/12Mn/1.6K	1.2	100Fe/13.9Mn/1.6K	1.2
Mn50	100Fe/50Mn/2.1K	1.2	100Fe/44.7Mn/2.0K	1.2
Mn100	100Fe/100Mn/2.9K	1.2	100Fe/92.8Mn/3.0K	1.3
Mn300	100Fe/300Mn/5.7K	1.2	100Fe/269.7Mn/5.8K	1.3
MnK	0Fe/100Mn/1.4K	1.2	0Fe/100Mn/1.4K	1.2

loaded. The samples were firstly heated in helium from room temperature to 500 °C, and then held for 1 h to remove moisture and other volatile impurity in the samples. The samples were subsequently cooled to 100 °C under the flow of He, and then exposed to CO_2 for half an hour. Followed by flushing with He for 1 h to remove the weakly adsorbed CO_2, the samples were finally heated to 500 °C at a rate of 6 °C/min in a flow of He and the TPD spectra were recorded.

Mössbauer spectroscopy was measured with a FAST Series MR-351 constant-acceleration Mössbauer spectrometer (FAST, Germany) at room temperature, using a 25 mCi ^{57}Co in Pd as γ-ray source. The spectrometer was operated in the symmetric constant acceleration mode. The spectra were collected over 512 channels in the mirror image format. Data analysis was performed using a nonlinear least square fitting routine that models the spectra as a combination of singlets, quadruple doublets and magnetic sextuplets based on a Lorentzian line shape profile. The spectral components were identified on the basis of their isomeric shift (IS), quadruple splitting (QS) and magnetic hyperfine field (Hhf). All isomer shift values were reported with respect to metallic iron (α-Fe). Magnetic hyperfine fields were calibrated with the 330 kOe field of α-Fe at room temperature.

2.3. Reactor system and operation procedure

FTS performances of the catalysts were tested in a 1 dm^3 continuous stirred tank reactor (CSTR). For each test, about 20 g fresh catalyst and 320 g liquid wax were loaded in the reactor. After being reduced at 270 °C with syngas (H_2/CO = 0.67) for 24 h, the reactor system was adjusted to the required reaction conditions. The detailed description of the reactor and product analysis systems have been given elsewhere [18].

3. Results and discussions

3.1. Crystallite structure of the fresh catalysts

The crystallite structures of the fresh catalyst were measured by XRD and Mössbauer spectroscopy. The XRD patterns and the Mössbauer parameters of the fresh catalysts are shown in figure 1 and table 2, respectively. The main phase of the fresh catalysts identified by XRD is hematite (α-Fe_2O_3). Simultaneously, the intensity of the diffraction peaks of α-Fe_2O_3 is gradually weakened with the increase of Mn content. The results of Mössbauer analysis (table 2) also show that the content of superparamagnetic (spm) Fe^{3+} ions, with the crystallite diameters smaller than 13.5 nm [25], increases with the incorporation of Mn promoter. At the same time, since the total potassium weight percent is equal in the present catalyst system, K/Fe ratio will increase with the increase of manganese content. Our previous study has found that the addition of

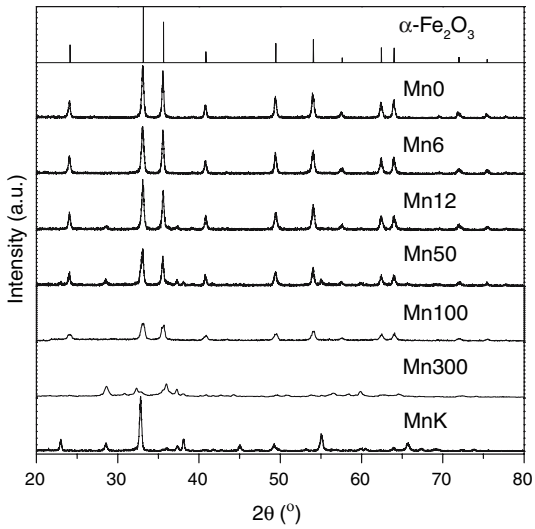

Figure 1. XRD patterns of the catalysts as-prepared.

potassium into Fe–Mn catalyst promoted the aggregation of α-Fe_2O_3, and the diffraction peak intensity of α-Fe_2O_3 increased with the incorporation of potassium [12]. However, it is found that the Mn promoter plays dominant role on the structure of the fresh catalyst in the present study. The addition of Mn promoter improves the dispersion of α-Fe_2O_3, and the crystallite size of α-Fe_2O_3 is decreased by the incorporated Mn. The study over Mn-promoted Fe/Silicate-1 catalyst by Das *et al.* [26] also revealed that the addition of Mn decreased the particle size of iron oxide. In addition, Mössbauer analysis also indicated that the hyperfine field (Hhf) of α-Fe_2O_3 in the Mn0 catalyst is 514 kOe, which comes up to the standard value (515 kOe) of α-Fe_2O_3 standard [12]. With the increase of Mn content, the Hhf value gradually decreases from 514 kOe to 486 kOe, which is due to the intro-incorporation of Fe^{3+} and Mn^{3+} ions in the lattices of α-Fe_2O_3 and α-Mn_2O_3 [24]. The result also implies that the Fe–Mn

Table 2
Mössbauer parameters of the catalysts as-prepared

Catalysts	Phases	MES parameters			
		IS (mm/s)	QS (mm/s)	Hhf (kOe)	Area (%)
Mn0	α-Fe_2O_3	0.37	−0.20	514	100.0
Mn6	α-Fe_2O_3	0.37	−0.21	510	96.5
	Fe^{3+}(spm)	0.26	0.94		3.5
Mn12	α-Fe_2O_3	0.37	−0.21	509	96.0
	Fe^{3+} (spm)	0.31	0.72		4.0
Mn50	α-Fe_2O_3	0.36	−0.21	507	87.2
	Fe^{3+} (spm)	0.35	0.76		12.8
Mn100	α-Fe_2O_3	0.37	−0.21	501	78.5
	Fe^{3+} (spm)	0.29	0.72		21.5
Mn300	α-Fe_2O_3	0.35	−0.04	486	45.0
	Fe^{3+} (spm)	0.33	0.82		55.0

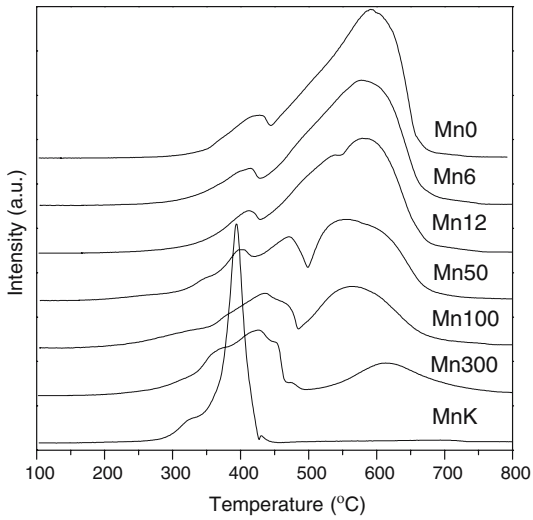

Figure 2. H_2-TPR profiles of the catalysts.

interaction is enhanced with the incorporated Mn promoter in the Fe–K catalyst system.

3.2. *Reduction behaviors of the catalyst in H_2 and CO*

Figure 2 displays the H_2-TPR profiles of the catalysts. The TPR profile of the Mn-free catalyst (Mn0) shows two distinct reduction peaks. The first peak centered at 428 °C represents the reduction of α-Fe_2O_3 to Fe_3O_4, and the second peak at 591 °C represents the further reduction of Fe_3O_4 to α-Fe [27]. The TPR profile of the Fe-free model catalyst (MnK) also shows two reduction peaks. The first peak at 328 °C can be attributed to the reduction of α-Mn_2O_3 to Mn_3O_4, and the second peak at 394 °C is to the further reduction of Mn_3O_4 to MnO [27]. The formed MnO phase can not be further reduced under the present conditions (< 500 °C) due to the thermodynamic reasons [24,27].

The TPR profile of the catalyst promoted with a low amount of Mn (Mn6) shows the similar reduction peaks with that of Mn0 sample. Compared with the TPR profiles of Mn0 and MnK, the first peak at low temperature represents the reduction of α-Fe_2O_3 and α-Mn_2O_3 to Fe_3O_4 and MnO, and the second peak at high temperature can be attributed to the further reduction of Fe_3O_4 to α-Fe. However, for the catalysts (Mn12 and Mn50) with middle amount of Mn, the high-temperature reduction peak is gradually separated into two distinct peaks, indicating the reduction of Fe_3O_4 to α-Fe via wustite (FeO) as an intermediate [27], which may be caused by the increase of Fe–Mn interaction with increasing Mn content. Thermodynamically, the wustite (FeO) phase is unstable below 590 °C, but the enhanced Fe–Mn interaction improves the incorporation of Mn^{2+} ions into the FeO lattice and stabilizes the wustite phase [24,25]. With the further increase of Mn content, for catalysts Mn100 and Mn300, the Fe–Mn interaction (the incorporation of Fe^{3+} and Mn^{3+} ions in their oxide lattices) is strongly enhanced, which shifts the first reduction peak to high temperature, and the former two reduction peaks are gradually united together, to form two distinct reduction regions in the whole TPR profile. The first reduction region at low temperature can be ascribed to the reduction of the mixed oxide formed by α-Fe_2O_3 and Mn_2O_3 to an (Fe, Mn)$_3O_4$ mixed oxide phase, which is further reduced to manganowustite, (Fe, Mn)O, by comparison with the TPR profiles of Mn0 and MnK [24,27]. The second reduction region is only associated with the reduction of (Fe, Mn)O to α-Fe and MnO, due to the reduction of α-Mn_2O_3 to MnO is below 500 °C [24,25,27]. It is found that the temperature of the two reduction peaks of the Mn6 catalyst is lower than that of the Mn-free catalyst (Mn0). However, the first reduction peaks become a big reduction region, and the latter reduction peak shifts to higher temperature with the further addition of Mn content. These results indicate that the addition of an appropriate amount of Mn can promote the catalyst reduction, however, the Fe–Mn interaction is strengthened and the Fe^{2+} ions are stabilitated during the H_2 reduction with the further addition of Mn promoter. As mentioned above, the XRD and MES results of the fresh catalyst implied that Mn promoter improves the dispersion of α-Fe_2O_3 and reduces its particle size. At the same time, the Fe–Mn interaction is also enhanced with the increased Mn incorporation. The Fe–Mn interaction is not strong and the main role of Mn promoter is to decrease the crystallite size of α-Fe_2O_3 with small amount of Mn promoter added, which promote the reduction, since the small crystallite size of α-Fe_2O_3 can be easily reduced in H_2 [28]. However, the Fe–Mn interaction is greatly strengthened with the further addition of Mn promoter, which results in the formation of mixed oxide ((Fe, Mn)$_3O_4$, (Fe, Mn)O) during H_2 reduction, making Fe^{2+} more stable and difficult to be further reduced.

The CO-TPR profiles of the fresh catalysts are presented in figure 3. All profiles show two distinct reduction/carburization peaks. The first peak may be attributed to the reductions of both α-Fe_2O_3 to Fe_3O_4 and α-Mn_2O_3 to MnO and the second peak represents the further reduction and carburization of iron oxide accompanying with partial carbon deposition as a result of Boudouard reaction ($2CO = C + CO_2$) [27,29]. The TPR profile of the MnK catalyst also presents two peaks, which is ascribed to the reduction of α-Mn_2O_3 to Mn_3O_4, and Mn_3O_4 to MnO, respectively [27]. The MnO phase can not be further reduced and carburized, and it also does not catalyze the Boudouard reaction [19,27]. The CO-TPR profile also indicated that the first peak firstly shifts to higher temperature with the increase of Mn content to 100Fe/50Mn. This may be attributed to that Mn promoter enhances the Fe–Mn interaction and stabilizes the Fe^{3+} ions as mentioned

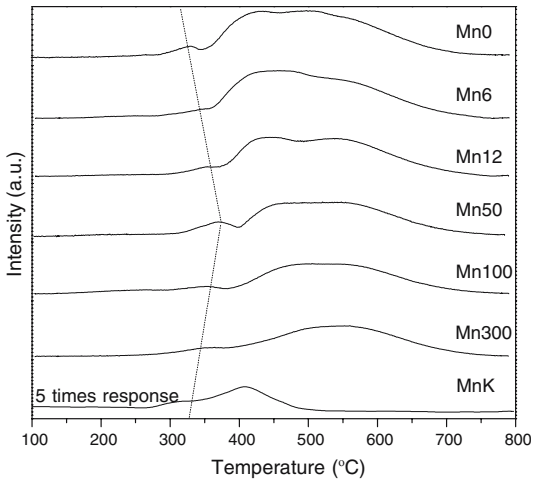

Figure 3. CO-TPR profiles of the catalysts.

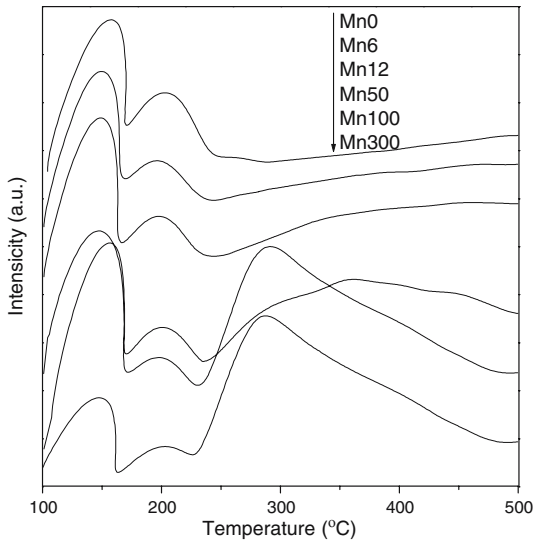

Figure 4. CO_2-TPD profiles of the catalysts.

above. However, the temperature of the first reduction peak gradually decreases with the further addition of Mn promoter, which may be ascribed to the high Mn content, since the reduction temperature of the α-Mn_2O_3 is lower than that of the α-Fe_2O_3 [25], by comparison with the TPR profiles of Mn0 and MnK. It is also found that second peak shifts to higher temperature, and the area of the second peak decreases with the incorporation of Mn promoter. The results imply that the addition of Mn promoter suppresses the catalyst carburization in CO. It has been proved that potassium can promote the carburization of the iron catalyst. As discussed previously, the addition of Mn restrains the further reduction and carburization of Fe_3O_4 and FeO phase, since the incorporation of Mn promoter enhances the Fe–Mn interaction, and Fe^{2+} ions are stabilized by the MnO phase. On the other hand, the crystallite size of α-Fe_2O_3 decreases with increasing Mn content, which also retards the carburization of catalyst [26].

3.3. Surface basicity of the catalyst

CO_2-TPD is often used to determine the surface basicity of solid materials [30]. The CO_2-TPD curves of the present catalysts are presented in figure 4. The amount of desorbed CO_2 and the temperature of maximum desorption of CO_2 are the indicators for the amount and strength of basic sites, respectively [31]. Three desorption peaks were observed in each TPD curve. The first peak at the temperature range of 100–160 °C corresponds to the desorption of CO_2 physically adsorbed, and the latter two peaks at the temperature range of 160–500 °C correspond to the desorption of CO_2 that interacts moderately with the surface basic sites [31,32]. More precisely, it is reasonable to assign the second peak to a bicarbonate species resulting from the interaction of CO_2 with basic hydroxyl groups of catalysts, which is corresponded to the weak surface basicity. The third peak may be attributed to a carbonate species and exhibits a higher thermal stability than hydrogen carbonate species [31,32], which is to the strong surface basicity. It is found that there is little change in temperature and area of the second peak with the increase of Mn content, the result implies that the variation of Mn content has few effects on the weak surface basicity of the catalyst. However, the third peak obviously shifts to a lower temperature, and the area of the desorption peak increases with the increase of Mn content. The result indicates that the strength of the strong basic sites is weakened and the amount of the strong basic sites is increased with the incorporated Mn promoter. A possible reason for the effect of Mn promoter on the catalyst surface basicity is that, the Mn–K interaction is strengthened with the addition of Mn promoter. This interaction suppresses the strong basicity of K on Fe–Mn–K catalyst, and leads to the decrease of the strength of the strong basic sites, since potassium presents a stronger surface basicity than manganese, and plays a critical role in improving the surface basicity [32]. At the same time, the amount of basic sites increases due to the increase of the total manganese weight in the catalyst, since manganese oxide also exhibits strong surface basicity [19].

3.4. Reduction and carburization behaviors in syngas

The XRD patterns and the Mössbauer parameters of the catalysts after reduction with syngas (H_2/CO = 0.67) at 270 °C, 0.3 MPa and 1000 h^{-1} for 24 h are summarized in figure 5 and table 3, respectively. Each XRD patterns (except for the Mn300 catalyst) shows a strong diffraction peak around 43°, which can be assigned to the overlap of iron carbide(s) with magnetite since most diffraction peaks of iron carbides reported in JCPDS database have prominent peaks

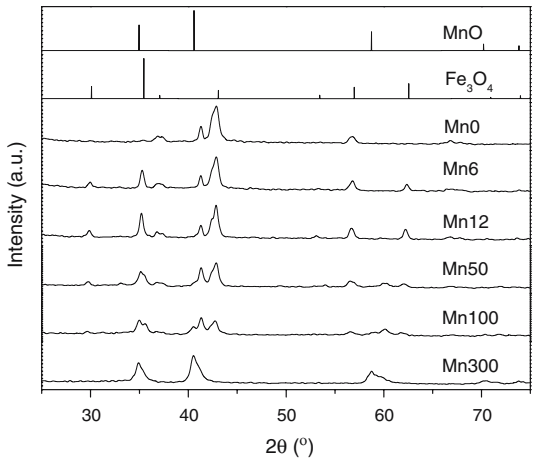

Figure 5. XRD patterns of the catalysts after reduction. Reduction condition: H_2/CO = 0.67, 270 °C, 0.3 MPa and 1000 h^{-1} for 24 h.

around 43°. It is found that the intensity of this peak decreases with the increase of manganese content. At the same time, it is also found that the intensity of the magnetite diffraction peak increases with the addition of small amount of Mn promoter. However, the XRD patterns mainly present the MnO diffraction peak, and its intensity increases with the further incorporation of Mn promoter. The Mössbauer parameters in table 3 show that the iron carbide(s) phases of the reduced catalyst is composed by χ-Fe_5C_2 and/or ε-Fe_2C, and the total iron carbide(s) content decreases with the increase of Mn content. On the other hand, the content of Fe_3O_4 in the reduced catalyst increases with the addition of Mn promoter. Moreover, the hyperfine field (Hhf) parameter of Fe_3O_4 for the Mn6 catalyst is closed to the standard value (490 kOe for Fe_3O_4 (A) and 440 kOe for Fe_3O_4 (B)) of pure magnetite. However, the Hhf parameter of Fe_3O_4 gradually decreases with the further

Table 3
Mössbauer parameters of the catalysts after reduction[a]

Catalysts	Phases	Mössbauer parameter				
		IS (mm/s)	QS (mm/s)	Hhf (kQe)	Area (%)	Degree of reduction (%)[b]
Mn0	χ-Fe_5C_2	0.30	−0.01	216	27.9	90.40
		0.35	0.04	184	8.9	
	ε-Fe_2C	0.23	−0.09	168	45.2	
		0.30	−0.11	130	7.4	
	Fe^{2+} (spm)	0.70	1.80		3.0	
	Fe^{3+} (spm)	0.30	0.80		7.6	
Mn6	χ-Fe_5C_2	0.30	−0.15	218	39.8	81.06
		0.35	−0.12	186	1.1	
	ε-Fe_2C	0.24	−0.12	168	36.7	
		0.30	−0.15	130	1.7	
	Fe_3O_4	0.35	−0.02	490	13.1	
		0.65	0.27	440	2.7	
	Fe^{3+} (spm)	0.30	0.80		5.0	
Mn12	χ-Fe_5C_2	0.30	−0.21	218	23.7	76.72
		0.35	0.17	186	4.5	
	ε-Fe_2C	0.24	−0.10	168	43.1	
		0.30	−0.06	130	3.1	
	Fe_3O_4	0.35	−0.04	490	16.8	
		0.65	−0.09	436	4.1	
	Fe^{3+} (spm)	0.30	0.80		4.7	
Mn50	χ-Fe_5C_2	0.30	−0.12	218	10.7	65.63
	ε-Fe_2C	0.24	−0.10	168	49.4	
		0.30	−0.28	130	3.3	
	Fe_3O_4	0.35	−0.09	481	19.6	
		0.60	0.09	435	1.3	
	Fe^{3+} (spm)	0.30	0.80		15.7	
Mn100	ε-Fe_2C	0.20	−0.04	174	34.3	41.50
		0.33	−0.19	123	4.4	
	Fe_3O_4	0.36	−0.04	473	21.0	
		0.58	−0.10	438	4.2	
	Fe^{3+} (spm)	0.43	0.81		36.1	
Mn300	Fe^{2+} (spm)	0.90	1.09		26.5	8.83
	Fe^{3+} (spm)	0..35	0.74		73.5	

[a] Reduction conditions: H_2/CO = 0.67, 270°C, 0.3 MPa and 1000 h^{-1} for 24 h.
[b] Degree of reduction $= \frac{A-B}{A} \times 100$ where A: the mole of oxygen in the iron compounds in the fresh catalyst; B: the mole of oxygen in the iron compounds in the reduced catalyst.

addition of Mn promoter. At the same time, the degree of reduction also decreases with increasing Mn content. As mentioned above, the addition of Mn promoter into the Fe–K catalyst system enhances the Fe–Mn interaction, which retards the carburization of the catalyst. The existence of MnO phase stabilizes the Fe_3O_4 phase by the incorporation of Mn^{2+} and $Fe^{2+}/(Fe^{3+})$ ions in the mixed oxide of $(Fe, Mn)_3O_4$, which presents a lower Hhf value and suppresses the further reduction and carburization of the catalyst, since Fe_3O_4 phase is susceptible to be carburized in syngas [15,24]. The role of Mn promoter to stabilize the Fe^{2+} and Fe^{3+} ions well agrees with the results of TPR and MES.

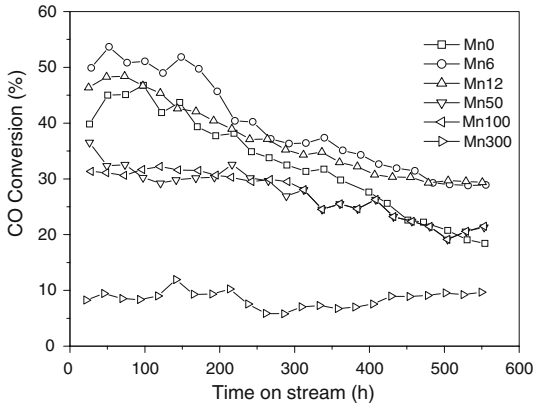

Fig. 6 Carbon monoxide conversion of the catalysts. Reaction condition: H_2/CO = 0.67, 250 °C, 1.50 MPa and 2000 h^{-1} for 550 h.

3.5. Fischer-Tropsch synthesis performance

The results of the effects of manganese promoter on catalyst activity, stability and selectivity for FTS are shown in table 4 and figure 6. It is found that the catalyst activity firstly increases with increasing Mn content, then passes through a maximum at a Mn/Fe weight ratio of 0.06, and finally decreases with further addition of Mn. At the same time, the addition of Mn decreases the deactivation rate. It is generally accepted that the iron carbides on catalysts surface are the main active phases for the FTS reaction [6,7], and so the amounts of active Fe sites on catalyst surface and the carburization extent of them play a crucial role in FTS activity. The present results may be caused by the synergetic effects of the follow factors: (1) Mn promoter improves the dispersion of active component Fe; (2) the addition of Mn promoter stabilizes the Fe^{2+} and Fe^{3+} ions, and suppresses the reduction and carburization of the catalyst in syngas; (3) the total iron content in the catalyst is decreased with the increases of Mn content. The synergetic effects of these factors result in an optimized amount of Mn promoter for the highest catalyst activity, as well as the increase of catalyst stability with increasing Mn content.

The effects of Mn promoter on the selectivity of hydrocarbon products are also shown in table 4. It is found that the selectivities to light products (C_2-C_{11}) firstly decrease, then pass through a minimum at a Mn/Fe weight ratio of 0.06, and finally increase with the increasing Mn content. The selectivities of the heavy products (C_{12}^{+}) show a controversy trend with that of light products.

1-Alkenes are the primary products of the FTS reaction over iron-based catalysts. Table 4 shows that the olefin selectivity of C_2-C_4 and C_5–C_{11} increases monotonically (from 74.8%, 74.0% to 89.2%, 81.7%, respectively) with increasing Mn content. Several factors maybe affect the present products selectivity. (1) The CO_2-TPD results suggest that Mn promoter weakens the strength of the strong basic sites. This would promote the formation of light hydrocarbons and saturated hydrocarbon, since higher surface basicity correlated

Table 4
Effects of manganese promoter on catalyst activity and selectivity[a]

Catalyst	Mn0		Mn6		Mn12		Mn50		Mn100		Mn300	
Time on stream (h)	315	530	315	530	312	529	312	530	315	531	309	530
CO conversion (%)	31.3	19.1	36.4	28.8	34.3	29.6	28.0	20.6	27.6	25.6	7.0	9.2
H_2+CO conversion (%)	30.8	19.2	35.6	28.8	33.1	29.2	27.1	20.4	26.8	25.0	8.0	10.1
Exit molar H_2/CO ratio	0.70	0.69	0.72	0.70	0.73	0.70	0.72	0.70	0.72	0.71	0.67	0.67
Extent of WGS ($P_{CO_2}P_{H_2}/(P_{CO}P_{H_2O})$)	4.63	2.37	6.98	4.80	6.78	4.63	4.93	3.26	4.75	4.09	0.82	0.80
Hydrocarbon selectivities (wt.%)												
CH_4	4.6	4.3	4.2	3.8	4.2	4.0	4.1	4.1	4.2	4.1	4.1	4.0
C_{2-4}	21.0	19.4	15.1	18.3	20.2	19.5	20.6	21.7	22.7	23.8	23.3	26.1
C_{5-11}	32.6	31.4	27.0	25.2	29.7	29.8	36.6	34.3	43.6	42.8	55.0	53.4
C_{12-18}	15.5	14.6	21.4	17.3	16.4	15.7	16.2	15.3	15.6	14.7	12.7	12.0
C_{19}^{+}	26.3	30.3.	32.3	35.4	29.5	31.0	22.5	24.6	13.9	14.6	4.9	4.5
Olefin selectivity (wt.%)												
C_{2-4}	74.5	74.8	75.2	75.9	78.9	80.5	82.7	83.3	82.5	82.8	88.7	89.2
C_{5-11}	73.3	74.0	74.6	75.5	76.8	76.6	78.5	78.3	78.4	78.9	81.1	81.7

[a] Reaction condition: H_2/CO = 0.67, 250°C, 1.50 MPa and 2000 h^{-1} for 550 h.

with a higher selectivity of heavy hydrocarbons and olefins [30]; (2) the amount of the strong basic sites is increased with incorporated Mn promoter, and leads to the increase of the heavy hydrocarbons and olefins selectivity, due to the amount of the basic sites also corresponds to the formation of heavy hydrocarbons and olefins [32]; (3) as-mentioned above, Mn promoter also improves the dispersion of the α-Fe_2O_3, reduces the crystallite size of it and enhances the Fe–Mn contact by the incorporation of iron and manganese atoms (ions) in mixed lattices during preparation and FTS performance. The interdispersion of iron and manganese atoms (ions) weakens the connection of carbon chain on the adjacent iron atoms and leads to the increase of light olefin selectivity [33]. The synergetic effects of these factors result in an appropriate amount of Mn promoter for the heavy hydrocarbons selectivity, as well as the increase of olefin selectivity with increasing Mn content. On the other hand, Das *et al*. [26] had reported that the Fe_3O_4 or (Fe, $Mn)_3O_4$ phase facilitates the formation of olefin. In the present study, the Fe_3O_4 or (Fe, $Mn)_3O_4$ phase is stabilized by the MnO phase, and the content of them is increased with the increase of Mn content, which maybe also lead to the increase of olefin selectivity.

4. Conclusions

Introduction of Mn promoter into the Fe–K catalyst system has significant influences on physico-chemical properties of the catalyst, such as the dispersion and crystallite size of α-Fe_2O_3, the interactions among iron, manganese and potassium, the reduction/carburization behaviors in H_2, CO and syngas, the surface basicity, the bulk phase structure of the catalyst, and the catalytic activity, stability and selectivity in FTS performance. Mn acts as a structural promoter as well as an electronic promoter when Mn and K coexisted in the iron-based catalyst system. The addition of Mn promoter improved the dispersion of the α-Fe_2O_3, and reduced the crystallite size of it. At the same time, the interaction of Fe-Mn and Mn–K was strengthened with the incorporation of Mn promoter, which stabilized Fe^{2+}, Fe^{3+} ions and the Fe_3O_4 phase, and suppressed the further reduction/carburization of them during the H_2, CO and syngas reduction process. In addition, Mn promoter decreased the deactivation rate of the catalyst in FTS reaction. Small amount of Mn promoter could enhance the catalyst activity, but the catalyst activity decreased with the further increase of Mn content. On the other hand, Mn promoter increased the amount of the strong basic sites and weakened the strength of the basic sites. The synergetic effects of the catalyst surface basicity and the interdispersion of iron atoms/ions with manganese oxide resulted in an appropriate of Mn for heavy hydrocarbons as well as the increase of olefin selectivity with increasing Mn content.

Acknowledgments

We gratefully acknowledge the financial support from Key Program of National Natural Science Foundation of China (20590361) and National Natural Science Foundation of Shanxi province (2006021014). This work was performed under the authority of Synfuels China Co., Ltd.

References

[1] H. Xiong, Y. Zhang, S. Wang and J. Li, Catal. Commun. 6 (2005) 512.
[2] Q. Ge, M. Neurock, H.A. Wright and N. Srinivasan, J. Phys. Chem. B. 106 (2002) 2826.
[3] M. Luo and B.H. Davis, Appl. Catal. A: Gen. 246 (2003) 171.
[4] B.H. Davis, Catal. Today 84 (2003) 83.
[5] W. Ngantsoue-Hoc, Y. Zhang, R.J. O'Brien, M. Luo and B.H. Davis, Appl. Catal. A: Gen. 236 (2002) 77.
[6] S. Li, S. Krishnamoorthy, A. Li, G.D. Meitzner and E. Iglesia, J. Catal. 206 (2002) 202.
[7] T.R. Motjope, H.T. Dlamini, G.R. Hearne and N.J. Coville, Catal. Today 71 (2002) 335.
[8] S. Li, R.J. O'Brien, G.D. Meitzner, H. Hamdeh, B.H. Davis and E. Iglesia, Appl. Catal. A: Gen. 219 (2001) 215.
[9] D.B. Bukur, X. Lang, D. Mukesh, W.H. Zimmerman, M.P. Rosynek and C. Li, Ind. Eng. Chem. Res. 29 (1990) 1588.
[10] D.B. Bukur, D. Mukesh and S.A. Patel, Ind. Eng. Chem. Res. 29 (1990) 194.
[11] M. Luo, R.J. O'Brien, S. Bao and B.H. Davis, Appl. Catal. A: Gen. 239 (2003) 111.
[12] Y. Yang, H. Xiang, Y. Xu, L. Bai and Y. Li, Appl. Catal. A: Gen. 266 (2004) 181.
[13] A.P. Raje, R.J. O'Brien and B.H. Davis, J. Catal. 180 (1998) 36.
[14] H.W. Pennline, M.F. Zarochak, J.M. Stencel and J.R. Diehl, Ind. Eng. Chem. Res. 26 (1987) 595.
[15] G.C. Maiti, R. Malessa, U. Löchner, H. Papp and M. Baerns, Appl. Catal. 16 (1985) 215.
[16] Y. Soong, V.U.S. Rao and R.J. Gormley, Appl. Catal. 78 (1991) 97.
[17] W.L. van Dijk, J.W. Niemantsverdriet, A.M. van der Kraan and H.S. van der Baan, Appl. Catal. 2 (1982) 273.
[18] L. Bai, H. Xiang, Li, Y. Han and B. Zhong, Fuel 81 (2002) 1577.
[19] K.B. Jensen and F.E. Massoth, J. Catal. 92 (1985) 98.
[20] J. Barrault and C. Renard, Appl. Catal. 14 (1985) 133.
[21] H.W. Pennline, M.F. Zarochak, R.E. Tischer and R.R. Schehl, Appl. Catal. 21 (1986) 313.
[22] J.J. Venter, A. Chen and M.A. Vannice, J. Catal. 117 (1989) 170.
[23] U. Lindner and H. Papp, Appl. Surf. Sci. 32 (1988) 75.
[24] G.C. Maiti, R. Malessa and M. Baerns, Appl. Catal. 5 (1983) 151.
[25] Y. Yang, H. Xiang, L. Tian, H. Wang, Zhang, Z. Tao, Y. Xu, B. Zhong and Y. Li, Appl. Catal. A: Gen. 284 (2005) 105.
[26] D. Das, G. Ravichandran and D.K. Chakrabarty, Catal. Today 36 (1997) 285.
[27] I.R. Leith and M.G. Howden, Appl. Catal. 37 (1988) 75.
[28] J.L. Rankin and C.H. Bartholomew, J. Catal. 100 (1986) 533.
[29] Y. Jin and A.K. Datye, J. Catal. 196 (2000) 8.
[30] M.E. Dry and G.J. Oosthuizen, J. Catal. 11 (1968) 18.
[31] S. Lee, J. Jang, B. Lee, J. Kim, M. Kang, M. Lee, M. Choi and S. Choung, J. Mol. Catal. A: Chem. 210 (2004) 131.
[32] C. Zhang, Y. Yang, B. Teng, T. Li, H. Zheng, H. Xiang and Y. Li, J. Catal. 237 (2006) 405.
[33] J. Abbot, N.J. Clark and B.G. Baker, Appl. Catal. 26 (1986) 141.